RSC Advances

Controlled Nitrogen Insertion in Titanium Dioxide for Optimal Photocatalytic Degradation of Atrazine

Journal:	*RSC Advances*
Manuscript ID:	RA-ART-01-2015-000890.R2
Article Type:	Paper
Date Submitted by the Author:	01-Apr-2015
Complete List of Authors:	Samsudin, Emy; University of Malaya, Nanocat Abd Hamid, Sharifah Bee; University of Malaya, Nanocat Ching, Juan; University of Malaya, Nanocat Basirun, Wan; University of Malaya, Chemistry; Institute of Postgraduate Studies, Nanotechnology & Catalysis Research Centre (NanoCat) Kandjani, Ahmad; RMIT University, School of Applied Sciences Bhargava, Suresh K; RMIT University, Centre for Advanced Materials and Industrial CHemistry (CAMIC) School of Applied Sciences (Applied Chemistry)

Controlled Nitrogen Insertion in Titanium Dioxide for Optimal Photocatalytic Degradation of Atrazine

Emy Marlina Samsudin[a], Sharifah Bee Abd Hamid[a,*], Joon Ching Juan[a], Wan Jefrey Basirun[a], Ahmad Esmaielzadeh Kandjani[b], Suresh K Bhargava[b]

[a]*Nanotechnology and Catalysis Research Center, University of Malaya, 50603 Kuala Lumpur, Malaysia*
[b]*Centre of Advanced Materials and Industrial Chemistry, RMIT University, Melbourne 3001, Australia*

* *Corresponding author.* Tel.: +60 379676959; fax: +60 379676956
Email address: sharifahbee@um.edu.my *(Sharifah Bee)*

Abstract

Introducing defects in intrinsic TiO_2 structural framework with nitrogen, enhanced the photocatalytic response towards the degradation of atrazine, as compared to undoped TiO_2. Both catalysts, prepared in an analogous manner demonstrated high crystallinity and well defined {100} facets dominant anatase, which serves as a pioneer platform for a good photocatalytic activity. The introduction of nitrogen increased the stability of the crystal structure which leads to the formation of pure active anatase phase. Although the optical response was shifted towards the visible region initiating the formation of new absorption defects and interstates energy level, the chemical state of nitrogen in doped TiO_2 controls the overall catalyst photoreactivity. In this study, it was found that surface area and degree of band gap reduction played a lesser role for photocatalysis enhancement, although it partly contributed, rather the concentration of surface charge traps and the type of structural framework formed during nitrogen incorporation. The enhancement in the photocatalytic degradation of atrazine clearly was influenced by the loading and doping nature of nitrogen dopant, which in turned, governed the type of chemical and optical properties of the final catalyst product.

Keywords: Photocatalysis, N-TiO_2, Doping, Visible light; Atrazine

Introduction

Since the green revolution introduced by Nobel laureate, Normal Borlaug in 1968, the usage of synthetic chemicals in maximizing crop productions increased rapidly and gave a significant impact towards decreasing the percentage of world starvation. However, despite the positive changes in sustaining the global needs, the green revolution had resulted in unintended serious public health and environmental issues *(1)*. Atrazine, an s-triazine group is a type of herbicides that is most commonly used in Malaysia to control the growth of broad leaf and grassy weeds *(2)* (Fig. 1). Due to the stable s-triazine ring of atrazine, it yields poor biodegradability and has great potential to leach through the soils and enters the ground water system *(3)*. According to Mc. Murray et al. *(4),* atrazine is repeatedly found in drinking water supplies and were detected above the recommended level of 0.1 ppb throughout European countries and the United States.

The technology for water pollutant abatement which includes absorption, ultrasonic destruction, microbial, chemical oxidation and filtration are effective to a certain degree of treatment, however, lacking the necessity to degrade very low pollutant concentrations. Atrazine are usually found in parts per billion levels in water sources and can be efficiently degraded into its harmless intermediates via photocatalysis. Unlike adsorption, the hazardous pollutants are destroyed rather than being transferred to another phase *(5)*. Photocatalysis also offers a more economical approach as there is no requirement for waste disposal, large energy usage and is less sensitive towards environmental change, i.e. pH of waste water.

The photocatalytic degradation of atrazine using 2.0 g/L of TiO_2 was intensively studied by Pellizzetti et al. *(3)* irradiated under solar lamp. The photocatalytic efficiency was proven as it took only 10 minutes to degrade 2 ppb of atrazine to less than 0.1 ppb. However, longer time was required for complete mineralization of the intermediates products. Following this discovery, many had attempted to degrade atrazine using TiO_2 nanoparticulate. C. Minero et al. *(6)* evaluated the photocatalytic degradation of 10 ppm atrazine using 0.2 g/L of TiO_2 suspensions and complete degradation was achieved in less than 120 min, I.K Konstantinou et al. *(7)* observed partial degradation of 10 ppm atrazine using 0.1 g/L of TiO_2 suspensions within half-lives ($t_{1/2}$) of 18.6 min, O. Zahraa et al. *(8)* degraded 10 ppm of atrazine using 1 g/L of TiO_2 suspensions and took 200 min for complete removal of atrazine and C.A Ruslimie et al. *(9)* evaluated the degradation of 5 ppm atrazine using 0.2 g/L TiO_2 and took more than 240 min for 70.6% atrazine degradation. The photocatalytic degradation of atrazine rate differs in each experiment and could be due to the different types of reactor configuration and TiO_2 synthesize method. Hence, an accurate evaluation of the photodegradation process could not be done. In all of these works, complete mineralization of atrazine was not observed, and a final stable end product of cyanuric acid was obtained.

One of the main factors that control the rate of photocatalytic degradation is the physicochemical properties of the catalyst used *(10-11)*. The application of intrinsic TiO_2 is limited due to the wide band gap which requires substantial amount of photons for electron/hole excitation *(12)*. Furthermore, the absorption efficiency of intrinsic TiO_2 covers only 4-5% of the UV region, leaving the major constituents of the solar light unharnessed *(13)*. Inducing defects into TiO_2 lattice using non-metal ions eliminates the drawbacks of doping using transition metals such as multiple charge carrier recombination centers within the band gap due to deep localized d states *(14-15)*. Nitrogen doped TiO_2 was initiated by Asahi et al. *(14),* where $TiO_{2-x}N_x$ films were prepared by sputtering TiO_2 in N_2(40%)/Ar gas mixture and subsequently annealed at 550°C in N_2 gas for 4 hours. The result showed the ability of $TiO_{2-x}N_x$ films to absorb lights below 500 nm, which was not observed for naked TiO_2 films. Furthermore, the hydrophilicity of $TiO_{2-x}N_x$ films was enhanced, an important criteria for a good photocatalyst system *(16)*. Many works in N-TiO_2 have since been reported (13, 17-21) concluding the positive effect of nitrogen incorporation into TiO_2 in terms of particles homogeneity, wider absorption of solar light, narrowing of band gap, alternative pathways for electron/hole recombination, retardation of crystal phase changes and enhanced photocatalytic degradation activity.

It is undeniable that successful preparation of N-TiO_2 photocatalyst generated successive visible-energy light conversion and improved its photocatalytic response in degrading organic pollutants. However, there is still a gap in understanding the factors which influences the photoactivity, especially by varying the concentration of nitrogen that enters the TiO_2 framework and creating either coordinated or substitutional doping. The degree of impurity imposed by introducing different loading of nitrogen was studied in this work, and was connected carefully to the photocatalytic degradation of atrazine. In addition, very little work aforementioned evaluated on the photodegradation of atrazine using N-TiO_2 and was discussed in this paper, followed by the degradation pathway and final formation of stable-end product of cyanuric acid.

Experimental

Materials

Titanium (IV) isopropoxide (TTIP, 97%), hydrochloric acid (37%), ethanol (95%), anhydrous ethanol (99%), triethylamine (99%) and atrazine (98%) were purchased from Sigma Aldrich. All chemical were used as received without further pre-treatment. Milli-Q deionized water was used throughout the whole experiment.

Synthesis of N-TiO_2

Five (different nitrogen loading content) of N-TiO_2 photocatalyst were synthesized using modified sol-gel method *(22)* and titanium (IV) isopropoxide (TTIP) as the metal precursor, pre-dissolved in anhydrous ethanol. Deionized water and hydrochloric acid in the molar ratio of 15:0.5 was added drop wise to obtain a clear sol, followed by the addition of triethylamine from an initial molar ratio of 0.5 to 2.5. The sol was left to age prior to solvent evaporation at 80°C overnight. The dried sol gels were further decomposed at 500 °C for 6 hours under constant air flow rate of 20 ml/min to obtain white N-TiO_2 powder. Similar method was employed for preparing un-doped TiO_2 without the addition of nitrogen precursor.

Characterization of N-TiO_2

The surface morphology and elemental composition of successful nitrogen doped in TiO_2 was observed with FESEM Quanta FEI 200F and energy dispersive x-ray spectroscopy (INCA Software). CHNS elemental analyzer (Perkin Elmer, 2400 series II) was also used to provide secondary information on the content of nitrogen successfully doped in TiO_2, using sulfamethazine (Sigma Aldrich) as the standard. The specific BET surface area and porosity were measured using multipoint nitrogen adsorption-desorption analyzer at relative pressure range of 0.01-0.90 P/P_o. The crystallinity and crystal phase of the samples was characterized by powder X-ray diffraction (XRD, Bruker AXS D8) using Cu Kα radiation. High resolution transmission electron microscopy (HR-TEM, JEM 2100-F) was performed at an accelerating voltage of 200kV was used to determine the microstructure of the catalyst. The samples were examined using 40 kV and 40 mA at a step size of 0.002 starting from 10° to 80°. The Raman spectra and photoluminescence (PL) measurement was performed using a LabRam confocal Raman microscope. Samples were excited by the 325 nm line of a continuous He–Cd laser at room temperature. Analysis of the functional group and types of chemical bonds was measured using Fourier Transformed Infra-red, FTIR Bruker Vertex 80/80v from 4000 to 400 cm^{-1}. The absorption edge of the prepared photocatalyst was measured using ultraviolet visible spectroscopy (Agilent, Cary 100) with a diffuse reflectance accessory. X-ray photoelectron spectroscopy (XPS) surface analyses were carried out using a flat gold (Si/10nm Ti/200nm Au) as the substrate and reference. Thermo Scientific K-alpha instrument with an un-monochromatized Mg Kα radiation (photon energy 1253.6 eV) source and vacuum better than 10^{-9} Torr as well as spectral resolution of 0.1 eV was used for XPS studies. XPS core levels were aligned to the C1s binding energy (BE) of 285 eV. The weight fractions of the crystal phase is calculated using Spurr equation of $f_A = 1/(1+1.26 \times I_R/I_A)$ where f_A is the weight fraction of anatase, $f_R = 1 - f_A$ is the weight fraction of rutile, I_A is the intensity of maximum anatase phase peak {101}, I_R is the intensity of maximum rutile phase peak {110} and 1.26 is the scattering coefficient *(23)*. For undoped TiO_2, the I_R and I_A is 5.57 and 108.44 respectively.

Photocatalytic Reactor and Degradation Activity

A custom built stirred tank photo-reactor (STR) consisting of six 250 ml quartz tube of equal dimensions were systematically arranged to received equal light intensity. The source of light was Xenon lamp (150W) with a UV light block filter ($\lambda < 420$ *nm*), positioned in the center of the reactor. The mass transfer between the photocatalyst and atrazine was enhanced via turbulent mixing at 450 rpm. Undoped TiO_2 and N-TiO_2 powder was used to degrade an initial atrazine concentration of 0.5 mg/L. The initial molar ratio of nitrogen in doped TiO_2 were 0.5, 1.0, 1.5, 2.0 and 2.5 with an initial catalyst loading of 0.5 g/L. Prior to the experiment, the photocatalyst were left in the aqueous suspension in darkness for 70 minute to achieved adsorption equilibrium between the catalyst and atrazine molecules. The experiment was treated in batch operation mode with a constant temperature maintained at 25±2°C. Throughout the experiments, 5.0 cm^3 of liquid samples were taken at various time intervals. The resultant aqueous solution was filtered prior to UV-Vis analysis (Perkin Elmer, Lambda 35). The average wavelength of atrazine used for UV-Vis analysis is 222.3 nm, with calibration coefficient, r^2 of 0.9998. The degradation efficiency, η was described using the equation [$\eta = (c_o-c)/c_o \times 100\% = (A_o-A)/A_o \times 100\%$]; where c_o and c/ A_o and A represents atrazine concentration/ absorption intensities at the initial and after photocatalytic activity for a certain time.

Intermediates Identification – LC/MS/MS

Atrazine degradation intermediates was determined using triple quadrupole liquid chromatography mass spectroscopy, LCMS/MS (Agilent 6400 Series) under electrospray ionization (ESI) and Zorbax StableBond-C18 reversed phase column (4.6 mm ID x 250 mm, 5 μm). A full scan mode (1 spectra/s) with a flow rate of 0.3 ml/min and runtime of 15 minute was used to determine the MS and MS/MS data. The mobile phase included filtered deionized water and acetonitrile at 9:1 volume ratio and the analysis was done under isocratic elution at pH 3.0.

Result and discussion

1. Characterization of N-TiO_2 powders

Morphology. Nitrogen was successfully introduced in TiO_2 in the range of 8-17 wt% as shown in Table 1. The nitrogen content in CHNS appeared slightly higher than by EDX, as CHNS measures the total bulk nitrogen while EDX measures the nitrogen presence on the surface of N-TiO_2. In both prepared catalyst, no change of color was observed and remained as white powder. This implies that the probability of coordinated nitrogen doping or chemisorbed γ-N_2 is present in TiO_2, as color changes is generally related to the red shift of the absorption edge due to substitutional doping *(24)*. The FESEM images of undoped and doped TiO_2 possessed agglomerates of spherical particles with an average particle diameter of 27 nm to 37 nm (Fig. 2). The EDX spectrum can be observed in Fig. 3. Although it was observed that N-precursor did not influence much on the size and shape of the particles, there was a slight increment of particle size for N-TiO_2 prepared at lower nitrogen loading. This could be partially due to the larger size of nitrogen atomic radius as compared to the oxygen atomic radius that occurred during dopant incorporation. This observation contradicts to the work done by M. Sathish et al. *(18),* where a significant decreased in the particle size was obtained after nitrogen doping. At higher nitrogen loading, the particles agglomeration appeared less, thus homogeneity and dispersibility of the particles was enhanced. This is clearly revealed in HR-TEM images (Fig. 4) where N1-TiO_2 appeared more dispersed as compared to N0-TiO_2. Both sample showed irregular crystal size ranging from 11 nm to 22 nm, where larger crystallite size was observed in doped TiO_2. The BET specific surface area and porosity presented in Table 2 showed less influence on the change of porosity after nitrogen doping, as compared to the specific surface area. The nitrogen absorption-desorption isotherms in Fig. 5 showed strong interaction of isotherm type IV and narrow distribution of uniform mesoporous pores in the range of 2 to 50 *(25).*

Crystallinity and Crystal Phase. XRD analysis was used to determine the crystallinity, crystal phase and weight fraction of each phase. Undoped TiO_2 consists of two crystal phase, namely anatase and rutile with mass ratio of 94:6 (Table 2). Interestingly, all doped TiO_2 showed predominant anatase phase and enhanced crystallinity under all synthesis condition. A major peak corresponding to {101} anatase phase was observed at angle 25°, followed by minor peaks at 37°, 47°, 54°, 55°, 62°, 69°, 70° and 75° and is based on JCPDS 731764 (Fig. 6). During the sol-gel process, the growth rate of the crystal exceeded the nucleation rate due to the addition of amine aqeuous solution which affects the overal pH of the solution. The presence of nitrogen in TiO_2 inhibits the condensation of spiral chain of anatase TiO_6 octahedral to linear chain of rutile TiO_6 octahedral. This can be seen from the disappearance of rutile major plane {110} at 27° angle after the addition of nitrogen. Similar observation was reported *(20)* whereby the addition of nitrogen improved the thermal stability of the catalyst by increasing the temperature required for rutile phase formation. It was further observed that the presence of nitrogen affects the full width of half maximum (FWHM), which is an indication of crystal size changes and possible lattice distortion (Fig. 7). At low nitrogen loading, there was a significant narrowing of FWHM, and the crystal size increased from 23 nm to 34 nm. The drastic change in the crystal size, however, did not affect the lattice spacing as shown in Table 2 *(26).* All crystallite size was calculated using Debye-Scherer's formula *(27)* using the highest intensity peak of the predominant phase.

Chemical Composition. RAMAN spectroscopy was employed to study the crystalline structure of undoped and doped TiO_2. All prepared catalyst showed significant anatase phase with major bands at 144 cm^{-1} (E_g), 395 cm^{-1} ($B1_g$), 515 cm^{-1} ($A1_g$) and 637 cm^{-1} ($E1_g$) (Fig. 8). A weak, but apparent Raman band of anatase was shown at 195 cm^{-1} (E_g). In all doped TiO_2, no remarkable rutile band at 446 cm^{-1} (E_g) was observed and supports the single crystal phase observed in the X-ray diffracion (XRD) spectrum. Although, 6 wt% of rutile phase was present in undoped TiO_2, no significant rutile band can be seen in the Raman spectra. This shows that Raman spectroscopy is suitable to identify the present of TiO_2 but not for distinguishing the different phases of anatase and rutile, especially at a low mass fraction. G. Yang et al. *(28)* prepared N-TiO_2 at different N:Ti atomic ratio using solvothermal method and obtained predominant anatase bands in the raman spectra. It was observed that the amount of nitrogen loaded in TiO_2 influences the size of the particles in a linear proportion. Larger particle size caused a blue shift towards a lower value of band in the raman spectra. Interestingly, in this work, the raman shifting patterns was similar to doped TiO_2 prepared below 11 wt% of nitrogen loading (Fig. 9). However, as nitorgen loading increased, red raman shift was observed, indicating smaller particles size. This observation is in good agreement with those shown in the XRD data. FTIR analysis was used to analyzed the presence of nitrogen in TiO_2 prior to doping at different loading. In Fig. 10a-b, similar spectra was observed in both undoped and doped TiO_2 around 2363-2360 cm^{-1} and 700-400 cm^{-1} which corresponds to absorbed CO_2 *(29)*, Ti-O stretching and Ti-O-Ti bridging stretching mode *(30).* The enlarged FTIR spectra from 1700 cm^{-1} to 1200 cm^{-1} revealed significant differences between both catalyst (Fig. 10c). Doped TiO_2 possessed multiple peaks within this region which corresponds to surfaced absorbed nitrogen at 1463-1384 cm^{-1} *(28)* and lattice nitrogen in the TiO_2 at 1632 cm^{-1}, 1546 cm^{-1}, 1338 cm^{-1} and 1255 cm^{-1} *(31).*

Chemical State. XPS analysis was used to determine the surface chemistry of the prepared photocatalyst. In Fig. 11, no nitrogen signal was detected in undoped TiO_2. The binding energy, E_g of N1s spectra was observed at 400.4 eV and no other E_g was present between 395 eV to 399 eV and above 400.4 eV. From previous work, interstitial nitrogen showed E_g around ~400 to 402 eV *(13,32),* 399.6 eV *(33)* and 399.8 eV *(34).* In addition, molecularly chemisorbed γ–N_2 shows Eg around ~400 to 402 eV (35). It is still debatious on the nature of N 1s present at E_g of ~400 to 402 eV, as whether nitrogen is doped intersitially or is present as chemisorbed N_2 or both. The difference of E_g and XPS intensity for each reported work were influenced by the selection of dopant *(20)* and catalyst preparation routes *(33)*. In this work, triethylamine was used as the source of nitrogen precursor. J. Ananpattarachai et al. *(20)* used similar dopant in preparing N-TiO_2 and obtained E_g at 402.5 eV, which was assigned to nitric oxide or nitrogen monoxide (NO) and nitrite (NO_2^-), corresponding to an interstitial doped nitrogen in TiO_2 due to the formed localised states with a π characteristics. L. Hu et al. (35) also incorporated triethylamine as N-precursor in synthesizing N-TiO_2. Interestingly, it was reported that the point of dopant introduction during the hydrolysis process determines the final state of N 1s formed in TiO_2. Molecularly chemisorbed N_2 are generally present if the crystallization process of TiO_2 occurs before the introduction of nitrogen and showed N 1s E_g around 400.5 and 401.4 eV while substitutited nitrogen in vice versa. As shown in Fig. 11, similar broad N1s XPS emission was also observed in other reported work (37-39), however strong corelation could not be made as different preparation procedures were employed. B. Viswanathan et al. (40) reviewed that low nitrogen loading in TiO_2 generally consists of Eg of N1s spectra within ~396-397 eV while for high nitrogen loading at ~400 eV, however no quantification was mentioned. In this work, the reported E_g of N1s peak at ~400.4 eV is attributed to the interstitial nitrogen in TiO_2 matrix with possible Ti-O-N or Ti-N-O linkages or chemisorbed molecular γ-N_2. For the latter, TiO_2 was doped at high nitrogen loading, however, no significant change in the crystal phase and lattice spacing was observed (Table 2). This indicates the presence of chemisorbed molecular γ-N_2 on the surface of TiO_2. As the amount of nitrogen doped in TiO_2 increased, the crystallinity of TiO_2 decreased. Observations made from FTIR (Fig. 10) supports the presence of probable Ti-O-N or Ti-N-O linkages as clear demarcation of lattice nitrogen is observed especially in the magnified FTIR spectrum from 1200 – 1700 cm^{-1}. N-H bond and NO_X are not presence in N1-TiO_2 due to the absency of E_g around 398.7 eV and above 403 eV respectively *(33).* This is further supported by the FTIR spectrum in Fig. 10c as no frequency of ammonia (N-H) was presenced. The probability of N-Ti-O lattice substitution can be ruled out as no E_g was observed below 397.5 eV, a characteristic of substituted nitrogen *(20).* Futhermore, a slight negative shift of E_g in Ti $2p_{3/2}$ between undoped TiO_2 and N-TiO_2 was observed in previous work when nitrogen substitutes for oxygen atom in a TiO_2 lattice *(41).* The change of E_g is due to the difference of electronegativity of nitrogen and oxygen atom in a N-Ti-O linkage, causing partial electron transformation from N to Ti as oxygen is more electronegative than nitrogen, thus increasing the electron density of Ti. However, this was not observed in this study hence the probability of substituted nitrogen in TiO_2 lattice is again eliminated. Based on Ti $2p$ spectra, the E_g of the photoelectron peak illustrates the existence of Ti^{4+} species in the TiO_2 nanostructures *(42).* The two deconvoluted O 1*s* peak remained unchanged for both undoped and doped TiO_2 at 530.0 eV and 531.7 eV. The former represents metallic oxide (Ti-O) and the latter represents surface hydroxyl, O_{OH} and is in agreement with the IR frequency observed in N0-TiO_2 and N1-TiO_2 at 3437.8 cm^{-1} and 3442 cm^{-1} respectively. No absorbed H_2O at ~532.7 eV was detected in the XPS peak *(43).* The presence of nitrogen in TiO_2 increased the number of hydroxyl sites and enhance the hydrophilicity of the catalyst. The hydroxyl peak in both FTIR (Fig. 10) and XPS (Fig. 11) analysis were more significant in N1-TiO_2 as compared to N0-TiO_2. In agreement with T. Morikawa et al. *(16);* the addition of nitrogen increased the wettability of the catalyst surface, thus compliments the photocatalytic activity.

Optical Properties. The UV-Vis spectra of undoped and doped TiO_2 catalyst prepared at different nitrogen loading are presented in Fig. 12. The corresponding band gap was obtained using Kubelka-Munk function *(34)* calculated using diffuse reflectance spectrum, with an indirect band gap coefficient of 0.5*(44)* (Table 2). A significant increased of light absorption towards lower photons energy level was observed for all doped TiO_2, extending the absorption coverage towards 400-550 nm of visible light region. This is due to the additional impurity level created within the band gap, thus causing a shift of the fermi level closer to the conduction band and consequence narrowing of band gap. This claim is further supported by Xiang et al. *(25),* whereby from first principle density functional theory (DFT) calculation, interstitial N-precursor can induced local states above the valence band and is responsible for the visible light response. According to B. Tian et al. *(29)*, the incorporation of nitrogen in the TiO_2 matrix forms a narrow N $2p$ band, which overlapped with O $2p$ orbital, promoting greater electrons mobility from the valence band to the conduction band during photoexcitation. However, no continuum interstates overlapping was observed in this work, as XPS data clearly shows no presence of substituted nitrogen in the TiO_2 lattice forming Ti-N-Ti linkages, but merely interstitial doping and chemisorbed γ-N_2. Apart from that, the formation of oxygen vacancies to compensate for overall charge balance played an important role towards the narrowing of the catalyst band gap as well. The formation of oxygen vacancies in doped TiO_2 compliments wider light absorptions above 500 nm *(45)* and is in good agreement with the blue shift of Ti $2p$ binding energy obtained in Fig. 11. Furtherance, the work done by H. Wu et al. *(46)* suggests that the formation of oxygen vacancy under nitrogen existence is easier to be formed as compared to naked TiO_2. Despite the remarkable improvement of photonic efficiency, the fate of electron and holes created during catalyst photoexcitation determines the overall photoactivity mechanism. The incorporation of nitrogen into TiO_2 shows broad visible emission around 530 nm, which consequently impacts the electron/hole recombination rate (Fig. 13). At high nitrogen loading, the photoluminescence intensity increases due to increasing number of oxygen vacancies and defect sites. Excessive oxygen vacancies acts as electron/hole recombination centre thus reduced the amount of active radicals generated and give rise to high photolumniscence intensity *(29).* It is observed that electron/hole recombination is inhibited at low nitrogen loading due to fewer charge trapping sites, hence facilitates better photocatalytic activity. In addition, the PL peak at 450 nm and 500 nm indicates defects presence in the doped TiO_2, and could act as a new adsorption centers *(47)* in the visible range, as N *2p* interstates overlapping with O *2p* responsible for vis-active was not observed in this study. Furthermore, the PL peaks shows a broad spectrum indicating the presence of oxygen vacancies, demonstrating not all of the nitrogen doped takes place in forming Ti-O-N or Ti-N-O linkages, but exists as amorphous nitrogen. This observation is supported by no change in the crystal structure as shown in Fig. 6.

Photocatalytic Activity

Decomposition of Atrazine under Visible Light. Prior to the photocatalytic degradation, the catalyst was left in the dark to reached absorption-desorption equilibrium (Fig. 14). In this study, 70 min was sufficient to reach the absorption-desorption saturation point. The surface area and porosity of the catalyst played an important role in controlling the amount of atrazine absorbed, as well as the surface charge of catalyst and substrate at the present pH. Relatively, higher absorption of atrazine was observed for undoped TiO_2 and highest loading of doped TiO_2 due to smaller particle size and greater porosity. (Table 2). However, these properties are not sufficient to justify the strength of a photocatalyst, and many other factors are involved such as morphology, crystal structure, optical and electronic properties *(48*). In addition, the catalyst surface charge is an important factor and is predominantly controlled by pH. The measured initial pH of atrazine solution is 7.5 and no further adjustment of pH was done throughout the experiment. In this condition, the charge of both catalysts is presumed as negatively charged as the isoelectric point of TiO_2 is from 6.25 to 6.90 *(24).* The attraction between the negatively charged catalyst and atrazine substrate was favored, as atrazine is protonated by the presence of H^+, thus facilitate the absorption of atrazine. In return, this provide a good combination for the photocatalytic activity as the generated electron/holes pair on the catalyst surface could readily reduce and oxidize absorbed atrazine into its degradation intermediates. As observed, the presence of nitrogen in TiO_2 significantly improved the photocatalytic degradation activity of atrazine, when compared to undoped TiO_2 (Fig. 15) under visible light irradiation. As shown in Fig. 15, the degradation rate constants are dependent on the amount of nitrogen loaded onto TiO_2, however, it does not represent a mathematical linear function. The function fits first order of reaction with coefficient, R^2= 0.98, whereby the rate of degradation is dependent on the loading of nitrogen (Fig. 16). Highest removal of atrazine was achieved less than 150 min at the lowest nitrogen loading in doped TiO_2. Higher nitrogen loading does not necessarily favor the photocatalytic reaction *(49)*due to the rapid electron/hole recombination as represented in Fig. 13, although absorption of atrazine during darkness was greater. This phenomenon explained the necessity of slow electron/hole recombination as well as enhanced photons absorption for a good photocatalysis process. Subsequently, undoped TiO_2 showed the weakest performance as the absorption of photons in the visible region is very poor, hence less light can be absorbed to generate active radicals for photodegradation.

Degradation Mechanisms. The intermediates for the photodegradation of atrazine were studied after 150 min of reaction using 0.5 g/L doped TiO_2. Based on LCMS/MS peaks, a total of 8 degradation intermediates were observed, which enables the plotting of potential degradation pathway (Fig. 17). The obtained *m/z* at 215.7 showed presence of atrazine even after 150 min of photodegradation activity and indicates incomplete removal of atrazine. The degradation pathway involved dehalogenation of chlorine at position two with a hydroxyl group, oxidation of alkyl side chain, further dealkylation and deamination. The degradation processes includes the formation of hydroxyatrazine, deethylatrazine,desethylhydroxyatrazine,deisopropylatrazine, deethyldeisopropylatrazine, ammelide and ammeline (3,4,6)and are listed in Table 3. The degradation pathway leads to a final amino group displacement with hydroxyl and formed a stable intermediate of cyanuric acid at *m/z* 129.1. I.K. Konstantinou et al. *(5)* referred the photodegradation mechanism of s-triazine as photo-Kolbe decarboxylation process, whereby similar pattern formation of alcohol, aldehyde and acid derivatives were observed.

Conclusion

Undoped and nitrogen doped TiO_2 were synthesized via sol gel technique using titanium (IV) isopropoxide and triethylamine as the source of Ti and N precursors respectively. A single anatase phase with less particles agglomeration was observed for all doped TiO_2. There was no dramatic change in the particle size of doped TiO_2 as the atomic radius of nitrogen atom is 6% larger than oxygen atomic radius. Based on the FTIR and XPS data, the hydrophilicity of TiO_2 surface increased in the presence of nitrogen, and is beneficial to any photocatalytic degradation of water pollutant. Nitrogen is doped interstitially forming Ti-O-N or Ti-N-O linkages, and induces local states 0.23 to 0.26 eV above the valence band which was responsible for the visible light response between 400 to 550 nm and effective narrowing of the band gap. In addition, no significant change in the crystal structure coupled with N1s XPS data and high nitrogen loading confirms the presence of chemisorbed γ-N_2 as well. In all prepared photocatalyst, doped TiO_2 with the lowest nitrogen loading yielded the highest rate of atrazine degradation, and superseded the performance of undoped TiO_2. At low nitrogen loading, the number of electron-hole trapping sites are hindered, which drives higher concentration of active radicals for atrazine degradation and mineralization. The degradation of atrazine followed first order rate of reaction, where the degradation activity is greatly influenced by atrazine concentration. The degradation pathway include dehalogenation of chlorine at position two with a hydroxyl group, oxidation of alkyl side chain, further dealkylation and deamination to form a stable non-toxic by product of cyanuric acid.

Acknowledgements

This research was funded by High Impact Research Grant (HIR-F000032) and IPPP Postgraduate Research Grant (PG062-2013B)

References

(1) D. Pimentel, "Green revolution agriculture and chemical hazards," *Sci. Total Environ.*, vol. 7, no. 188, pp. 86–98, 1996.

(2) A. Ahmad, L. Tan, and S. Abd Shukor, "Dimethoate and atrazine retention from aqueous solution by nanofiltration membranes.," *J. Hazard. Mater.*, vol. 151, no. 1, pp. 71–7, Feb. 2008.

(3) E. Pelizzeti, V. Mauriono, C. Minero, V. Carlin, E. Pramauro, O. Zerbinati, and M. L. Tosato, "Photocatalytic Degradation of Atrazine and Other s-Triazine Herbicides," *Environ. Sci. Technol.*, no. 20, pp. 1559–1565, 1990.

(4) T. Mc Murray, P. Dunlop, and J. Byrne, "The photocatalytic degradation of atrazine on nanoparticulate TiO_2 films," *J. Photochem. Photobiol. A Chem.*, vol. 182, no. 1, pp. 43–51, Aug. 2006.

(5) I. K. Konstantinou and T. A. Albanis, "Photocatalytic transformation of pesticides in aqueous titanium dioxide suspensions using artificial and solar light : intermediates and degradation pathways," *Appl. Catal. B Environ.*, vol. 42, pp. 319–335, 2003.

(6) C. Minero, E. Pelizzetti, S. Malato, and J. Blanc, "Large solar plant photocatalytic water decontamination : Degradation of atrazine," *Sol. Energy*, no. 5, pp. 411–419, 1996.

(7) I. K. Konstantinou, T. M. Sakellarides, V. A. Sakkas, and T. A. Albanis, "Photocatalytic Degradation of Selected s-Triazine Herbicides and Organophosphorus Insecticides over Aqueous TiO_2 Suspensions," *Environ. Sci. Technol.*, vol. 35, no. 2, pp. 398–405, 2001.

(8) O. Zahraa, L. Sauvanaud, G. Hamard, and M. Bouchy, "Kinetics of atrazine degradation by photocatalytic process in aqueous solution," *Int. J. Photoenergy*, vol. 05, no. 14, pp. 87–93, 2003.

(9) C. A. Ruslimie, H. Razali, and W. M.Khairul, "Catalytic Study on TiO_2 Photocatalyst Synthesised Via Microemulsion Method on Atrazine," *Sains Malaysiana*, vol. 40, no. 8, pp. 897–902, 2011.

(10) Q. Chen, H. Shi, W. Shi, Y. Xu, and D. Wu, "Enhanced visible photocatalytic activity of titania–silica photocatalysts: effect of carbon and silver doping," *Catal. Sci. Technol.*, vol. 2, no. 6, p. 1213, 2012.

(11) H. S. Kibombo, R. Peng, S. Rasalingam, and R. T. Koodali, "Versatility of heterogeneous photocatalysis: synthetic methodologies epitomizing the role of silica support in TiO2 based mixed oxides," *Catal. Sci. Technol.*, vol. 2, no. 9, p. 1737, 2012.

(12) Y. Alivov, V. Singh, Y. Ding, L. J. Cerkovnik, and P. Nagpal, "Doping of wide-bandgap titanium-dioxide nanotubes: optical, electronic and magnetic properties.," *Nanoscale*, vol. 6, no. 18, pp. 10839–49, Sep. 2014.

(13) S. J. Darzi, A. R. Mahjoub, and S. Sarfi, "Visible-Light-Active Nitrogen Doped TiO_2 Nanoparticles Prepared by Sol-Gel Acid Catalyzed Reaction," *Iran. J. Mater. Sci. Eng.*, vol. 9, no. 3, pp. 17–23, 2012.

(14) R. Asahi, T. Morikawa, T. Ohwaki, K. Aoki, and Y. Taga, "Visible-light photocatalysis in nitrogen-doped titanium oxides.," *Science (80).*, vol. 293, no. 5528, pp. 269–71, Jul. 2001.

(15) A. S. Weber, A. M. Grady, and R. T. Koodali, "Lanthanide modified semiconductor photocatalysts," *Catal. Sci. Technol.*, vol. 2, no. 4, p. 683, 2012.

(16) T. Morikawa, R. Asahi, T. Ohwaki, K. Aoki, K. Suzuki, and Y. Taga, "Visible-light Photocatalyst - Nitrogen-doped Titanium Dioxide," *Research Report for R&D Review of Toyota CRDL*, vol. 40, no.3, pp. 45-50, 2005.

(17) M. Mrowetz, W. Balcerski, A. J. Colussi, M. R. Hoffmann, C. Fisica, and V. Uni, "Oxidative Power of Nitrogen-Doped TiO_2 Photocatalysts under Visible Illumination," *J. Org. Chem.*, vol. 108, no. 45, pp. 17269–17273, 2004.

(18) M. Sathish, B. Viswanathan, R. P. Viswanath, and C. S. Gopinath, "Synthesis , Characterization, Electronic Structure, and Photocatalytic Activity of Nitrogen-Doped TiO_2 Nanocatalyst," *Chem. Mater.*, vol. 17, no. 10, pp. 6349–6353, 2005.

(19) Y. U. Huang, Z. Xuxu, Y. I. N. Zhongyi, and T. A. O. Feng, "Preparation of Nitrogen-doped TiO_2 Nanoparticle Catalyst and Its Catalytic Activity under Visible Light *," *Chi*, vol. 15, no. 6, pp. 802–807, 2007.

(20) J. Ananpattarachai, P. Kajitvichyanukul, and S. Seraphin, "Visible light absorption ability and photocatalytic oxidation activity of various interstitial N-doped TiO_2 prepared from different nitrogen dopants," *J. Hazard. Mater.*, vol. 168, no. 1, pp. 253–61, Aug. 2009.

(21) K. Zhao, Z. Wu, R. Tang, and Y. Jiang, "Preparation of Highly Visible-Light Photocatalytic Active N-Doped TiO_2 Microcuboids," *J. Korean Chem. Soc.*, vol. 57, no. 4, pp. 489–492, 2013.

(22) X. Chen, L. Liu, P. Y. Yu, and S. S. Mao, "Increasing solar absorption for photocatalysis with black hydrogenated titanium dioxide nanocrystals.," Feb. 2011.

(23) S. C. Padmanabhan, S. C. Pillai, J. Colreavy, S. Balakrishnan, D. E. Mccormack, T. S. Perova, Y. Gun, S. J. Hinder, and J. M. Kelly, "A Simple Sol - Gel Processing for the Development of High-Temperature Stable Photoactive Anatase Titania," *Chem. Mater.*, vol. 19, no. 11, pp. 4474–4481, 2007.

(24) J. Sun, L. Qiao, S. Sun, and G. Wang, "Photocatalytic degradation of Orange G on nitrogen doped TiO_2 catalysts under visible light and sunlight irradiation.," *J. Hazard. Mater.*, vol. 155,no. 1–2, pp. 312–9, Jun. 2008.

(25) Q. Xiang, J. Yu, W. Wang, and M. Jaroniec, "Nitrogen self-doped nanosized TiO_2 sheets with exposed {001} facets for enhanced visible-light photocatalytic activity.," *Chem. Commun. (Camb).*, vol. 47, no. 24, pp. 6906–8, Jun. 2011.

(26) J.-Y. Bae, T.-K. Yun, K.-S. Ahn, and J.-H. Kim, "Visible-photoresponsive Nitrogen-Doped Mesoporous TiO_2 Films for Photoelectrochemical Cells," *Bull. Korean Chem. Soc.*, vol. 31, no. 4, pp. 925–928, Apr. 2010.

(27) Chaudhary V, Srivastava AK, Kumar J. On the Sol-gel Synthesis and Characterization of Titanium Oxide Nanoparticles. *Mater. Res. Soc.*, vol. 1352, pp. 10–24, May 2011**.**

(28) G. Yang, Z. Jiang, H. Shi, T. Xiao, and Z. Yan, "Preparation of highly visible-light active N-doped TiO_2 photocatalyst," *Chinese J. Chem. Eng.*, vol. 2015, no. 25, p. 5301, 2010.

(29) B. Tian, Y. Qian, B. Hu, J. Sun, and Z. Du, "Synthesis and characterization of nitrogen-doped titanium dioxide nanomaterials derived from nanotube sodium titanate precursor," *J. Mater. Res.*, vol. 27, no. 18, pp. 2408–2416, Aug. 2012.

(30) A. A. Umar, M. Yusri, A. Rahman, S. K. Saad, and M. M. Salleh, "Effect of NH3 Concentration on the Performance of Nitrogen doped TiO_2 Photoelectrochemical Cell," *Int. J. Electrochem. Sci.*, vol. 7, pp. 7855–7865, 2012.

(31) S. Livraghi, M. C. Paganini, E. Giamello, A. Selloni, C. Di Valentin, G. Pacchioni, V. P. Giuria, P. U. V, and V. R. Cozzi, "Origin of Photoactivity of Nitrogen-Doped Titanium Dioxide under Visible Light," *J. Am. Chem. Soc.*, vol. 128, no. 21, pp. 15666–15671, 2006.

(32) A. V. Emeline, V. N. Kuznetsov, V. K. Rybchuk, and N. Serpone, "Visible-Light-Active Titania Photocatalysts: The Case of N-Doped TiO_2s—Properties and Some Fundamental Issues," *Int. J. Photoenergy*, no. 258394, pp. 1–19, 2008.

(33) J. Wang, D. N. Tafen, J. P. Lewis, Z. Hong, A. Manivannan, M. Zhi, M. Li, and N. Wu, "Origin of Photocatalytic Activity of Nitrogen-Doped TiO_2 Nanobelts," *J. Am. Chem. Soc.*, vol. 131, pp. 12290–12297, 2009.

(34) Khalid NR, Ahmed E, Hong Z, Zhang Y, Ahmad M. "Nitrogen doped TiO_2 nanoparticles decorated on graphene sheets for photocatalysis applications," *Curr Appl Phys*. 2012;12(6):1485-1492.

(35) L. Hu, J. Wang, J. Zhang, Q. Zhang, and Z. Liu, "An N-doped anatase/rutile TiO2 hybrid from low-temperature direct nitridization: enhanced photoactivity under UV-/visible-light," *RSC Adv.*, vol. 4, no. 1, pp. 420–427, 2014.

(36) T. M. Orikawa, R. A. Sahi, and T. O. Hwaki, “Band-Gap Narrowing of Titanium Dioxide by Nitrogen Doping,” *Japan Soc. Appl. Phys.*, vol. 40, no. 6A, pp. 561–563, 2001.

(37) H. Irie, Y. Watanabe, and K. Hashimoto, “Nitrogen-Concentration Dependence on Photocatalytic Activity of $TiO_{2-x}N_x$ Powders,” *J. Phys. Chem. B*, vol. 107, pp. 5483–5486, 2003.

(38) Y. Nosaka, M. Matsushita, J. Nishino, and A. Y. Nosaka, “Nitrogen-doped titanium dioxide photocatalysts for visible response prepared by using organic compounds,” *Sci. Technol. Adv. Mater.*, vol. 6, pp. 143–148, 2005.

(39) Y. Lin, C. Weng, H. Hsu, Y. Lin, and C. Shiesh, “The Synergistic Effect of Nitrogen Dopant and Calcination Temperature on the Visible-Light-Induced Photoactivity of N-Doped TiO_2,” *Int. J. Photoenergy*, no. 268723, pp. 1–13, 2013.

(40) B. Viswanathan and K. R. Krishanmurthy, “Nitrogen Incorporation in TiO_2: Does It Make a Visible Light Photo-Active Material?,” *Int. J. Photoenergy*, no. 269654, pp. 1–10, 2012.

(41) Y. Cong, J. Zhang, F. Chen, and M. Anpo, “Synthesis and Characterization of Nitrogen-Doped TiO_2 Nanophotocatalyst with High Visible Light Activity,” *J. Phys. Chem. C*, no. 111, pp. 6976–6982, 2007.

(42) J. L. Sullivan and I. Bertoti, “Effect of ion and neutral sputtering on single crystal TiO_2,” *Vacuum*, vol. 42, no. 18, p. 1203, 1991.

(43) F. Dong, Y. Sun, and M. Fu, “Enhanced Visible Light Photocatalytic Activity of Cluster Modified N-Doped for Degradation of Toluene in Air,” *Int. J. Photoenergy*, no. 569719, pp. 1–10, 2012.

(44) U. Pal, E. S. Mora, and A. E. Morales, “Use of diffuse reflectance spectroscopy for optical characterization of un-supported nanostructures,” *Rev. Mex. Fis.*, vol. 53, no. 5, pp. 18–22, 2007.

(45) W. Zhang, L. Zou, R. Lewis, and D. Dionysio, “A Review of Visible-Light Sensitive TiO_2 Synthesis via Sol-Gel N-Doping for the Degradation of Dissolved Organic Compounds in Wastewater Treatment,” *J. Mater. Sci. Chem. Eng.*, vol. 2, pp. 28–40, 2014.

(46) H. Wu, Y. Lin, and S. Lin, “Mechanisms of Visible Light Photocatalysis in N-Doped Anatase TiO_2 with Oxygen Vacancies from GGA + U Calculations,” *Int. J. Photoenergy*, no. 289328, pp. 1–7, 2013.

(47) D. Li, H. Haneda, S. Hishita, N. Ohashi, and N. K. Labhsetwar, “Fluorine-doped TiO_2 powders prepared by spray pyrolysis and their improved photocatalytic activity for decomposition of gas-phase acetaldehyde,” *J. Fluor. Chem.*, vol. 126, pp. 69–77, 2005.

(48) T. Mishra, M. Mahato, N. Aman, J. N. Patel, and R. K. Sahu, “A mesoporous W,N co-doped titania nanomaterial with enhanced photocatalytic aqueous nitrate removal activity under visible light,” *Catal. Sci. Technol.*, vol. 1, no. 4, p. 609, 2011.

(49) S. Bingham and W. A. Daoud, “Recent advances in making nano-sized TiO_2 visible-light active through rare-earth metal doping,” *J. Mater. Chem.*, no. 21, pp. 2041–2050, 2011.

Caption of Figures

Fig. 1. Atrazine molecular structure

Fig. 2. FESEM images of a) N0-TiO_2, b) N1-TiO_2, c) N3-TiO_2 and d) N5-TiO_2 taken at 50,000x magnification

Fig. 3. EDX spectrum of N0-TiO_2 and N1-TiO_2

Fig. 4. HR-TEM images of TiO_2 powders for a) N0-TiO_2, b) N1-TiO_2 and c) lattice spacing of anatase phase for N1-TiO_2

Fig. 5. Nitrogen adsorption-desorption linear isotherm (Type IV) for a) N0-TiO_2 and b) N1-TiO_2

Fig. 6. XRD spectra showing the crystal structure of a) N0-TiO_2, b) N1-TiO_2, c) N2-TiO_2, d) N3-TiO_2, e) N4-TiO_2 and f) N5-TiO_2

Fig. 7. Effect of FWHM, crystallite size and band gap alterations at different loading of nitrogen in TiO_2

Fig. 8. Raman spectra of a) N0-TiO_2, b) N1-TiO_2, c) N2-TiO_2, d) N3-TiO_2, e) N4-TiO_2 and f) N5-TiO_2

Fig. 9. Raman localized spectra of a) N0-TiO_2, b) N1-TiO_2, c) N2-TiO_2, d) N3-TiO_2, e) N4-TiO_2 and f) N5-TiO_2

Fig. 10. FTIR spectra of a) N0-TiO_2, b) N1-TiO_2 and c) enlarged FTIR spectra of Fig. 10b) from 1200cm^{-1} to 1700 cm^{-1}

Fig. 11. XPS Spectra of N 1*s*, Ti 2*p* and O 1*s* of N0-TiO_2 and N1-TiO_2

Fig. 12. a)Absorption spectrum and b) localized absorption spectrum for all prepared photocatalyst at different nitrogen loading

Fig. 13. Photoluminescence spectrum for for all prepared photocatalyst at different nitrogen loading

Fig. 14. Absorption-desorption profile of atrazine in darkness for all prepared photocatalyst at different nitrogen loading

Fig. 15. Percentage removal of atrazine and its corresponding rate constant for all prepared photocatalyst at different nitrogen loading

Fig. 16. First order rate of reaction graph of TiO_2 doped with nitrogen (r^2 coefficient > 98%)

Fig. 17. Proposed degradation pathway of atrazine using TiO_2 doped with nitrogen

Fig. 1

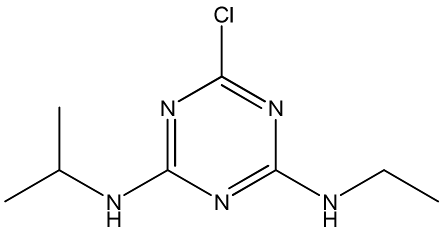

Fig. 1. Atrazine molecular structure

Fig. 2

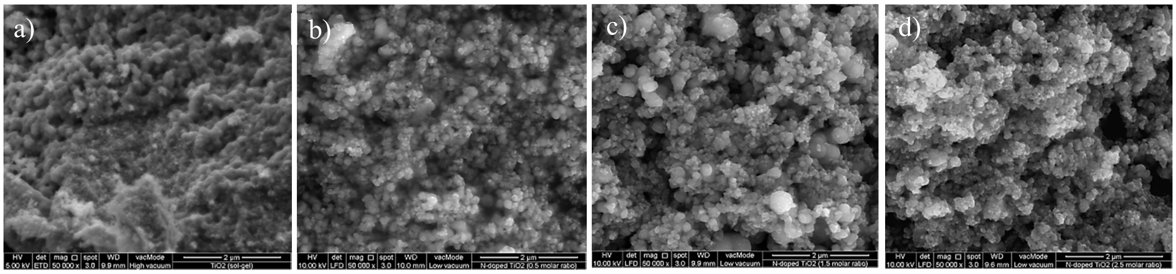

Fig. 2. FESEM images of a) N0-TiO_2, b) N1-TiO_2, c) N3-TiO_2 and d) N3-TiO_2 taken at 50,000x magnification

Fig. 3

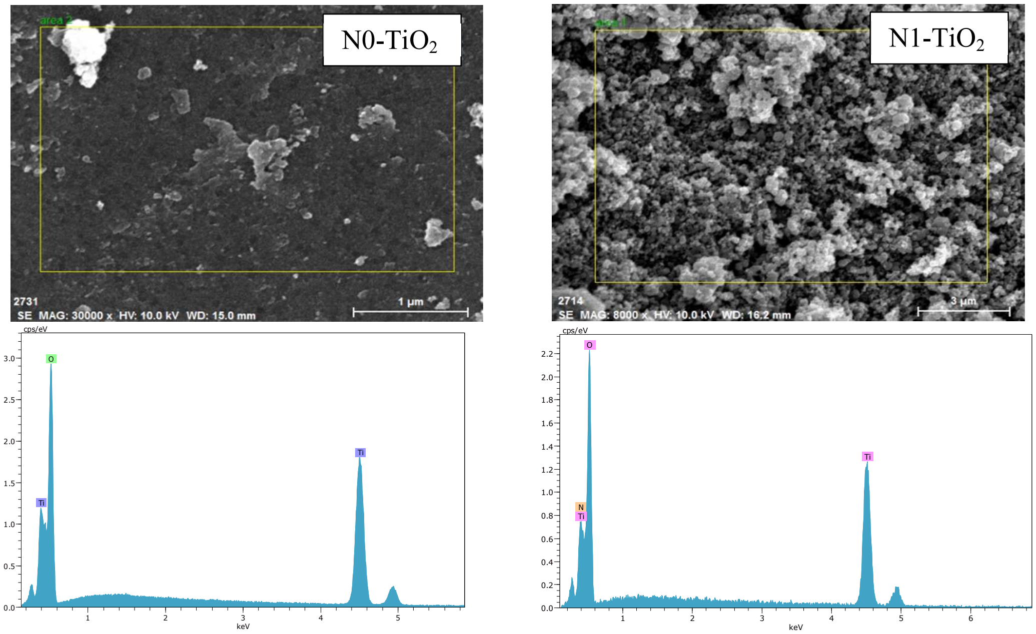

El	AN	Series	unn. C [wt%]	C. norm [wt%]
O	8	K-series	48.48	41.75
Ti	22	K-series	67.63	58.25
			116.12	100.00

El	AN	Series	unn. C [wt%]	C. norm [wt%]
N	7	K-series	10.14	8.71
O	8	K-series	44.32	38.04
Ti	22	K-series	62.05	53.25
			116.51	100.00

Fig. 3. EDX spectrum of N0-TiO$_2$ and N1-TiO$_2$

Fig. 4

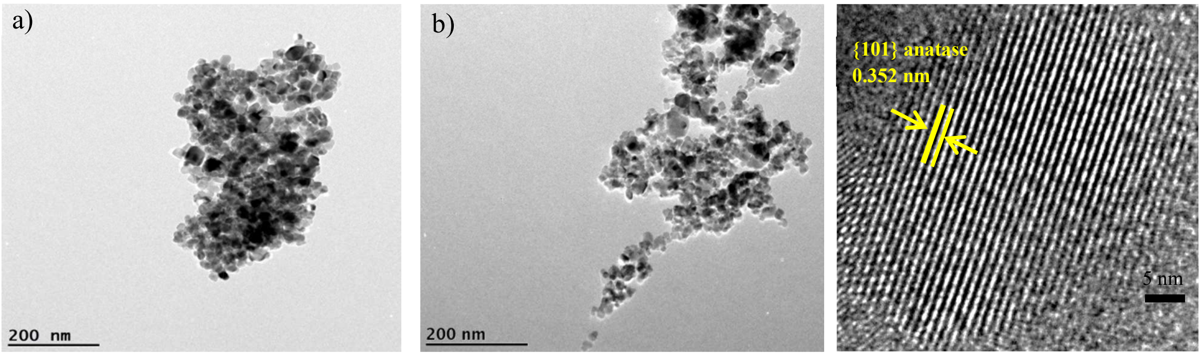

Fig. 4. HR-TEM images of TiO$_2$ powders for a) N0-TiO$_2$, b) N1-TiO$_2$ and c) lattice spacing of anatase phase for N1-TiO$_2$

Fig. 5

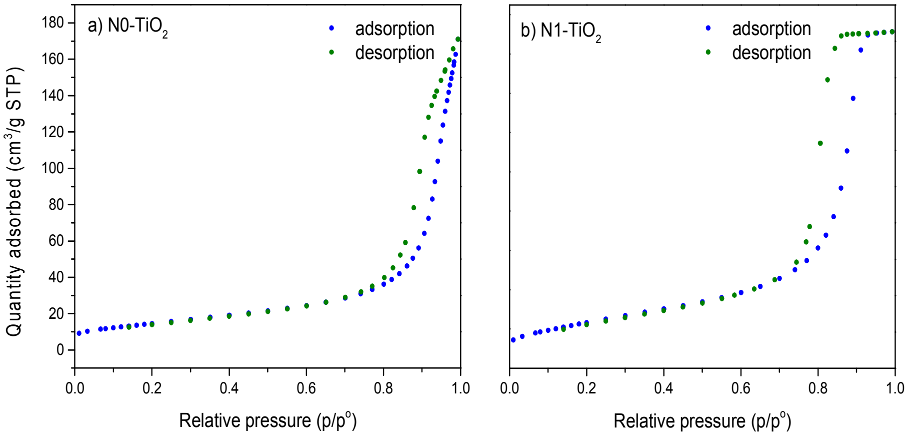

Fig. 5 Nitrogen adsorption-desorption linear isotherm (Type IV) for all a) N0-TiO_2 and b) N1- TiO_2

Fig. 6

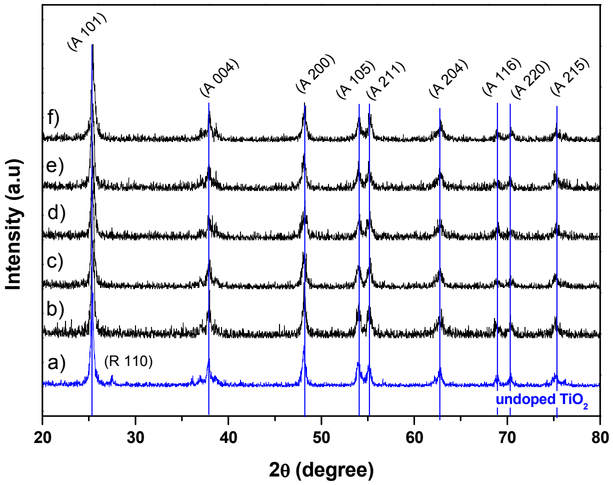

Fig. 6. XRD spectra showing the crystal structure of a) N0-TiO_2, b) N1-TiO_2, c) N2-TiO_2, d) N3-TiO_2, e) N4-TiO_2 and f) N5-TiO_2

Fig. 7

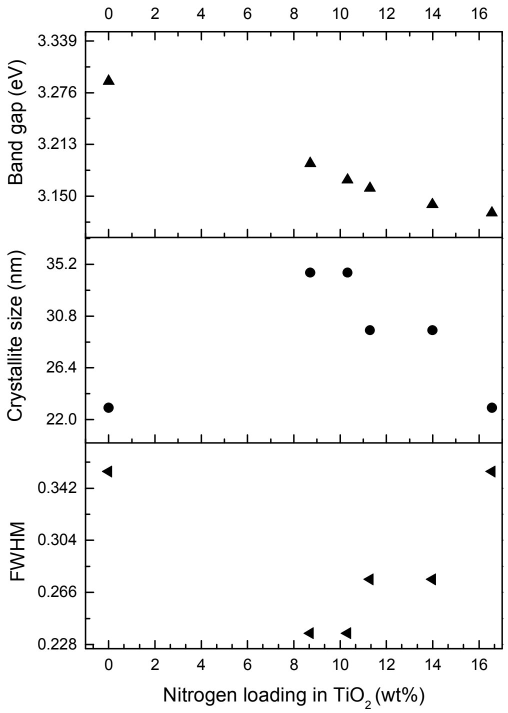

Fig. 7. Effect of FWHM, crystallite size and band gap alterations at different loading of nitrogen in TiO$_2$

Fig. 8

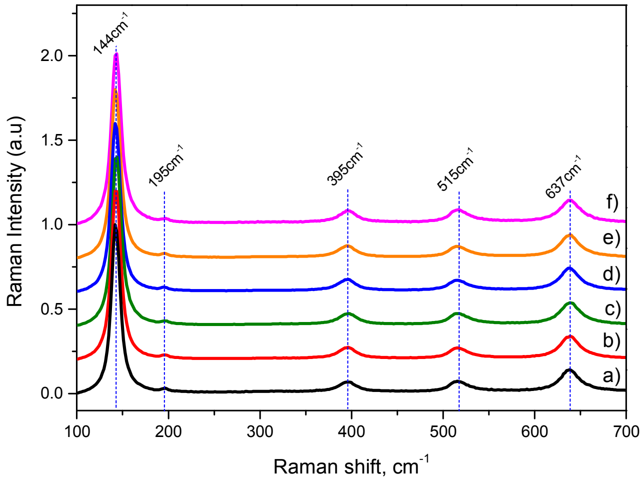

Fig. 8. Raman spectra of a) N0-TiO$_2$, b) N1-TiO$_2$, c) N2-TiO$_2$, d) N3-TiO$_2$, e) N4-TiO$_2$ and f) N5-TiO$_2$ TiO$_2$

Fig. 9

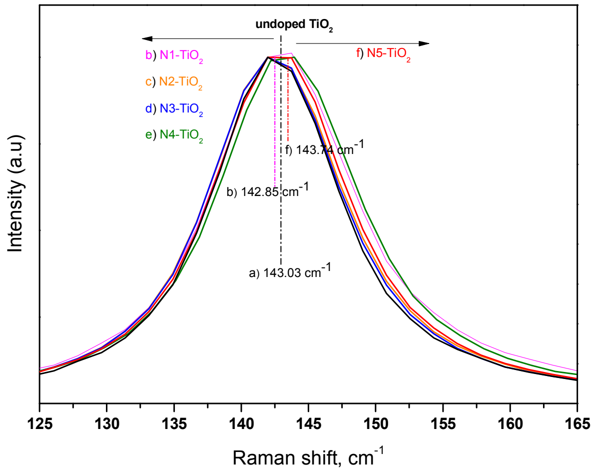

Fig. 9. Raman localized spectra of a) N0-TiO_2, b) N1-TiO_2, c) N2-TiO_2, d) N3-TiO_2, e) N4-TiO_2 and f) N5-TiO_2 TiO_2

Fig. 10

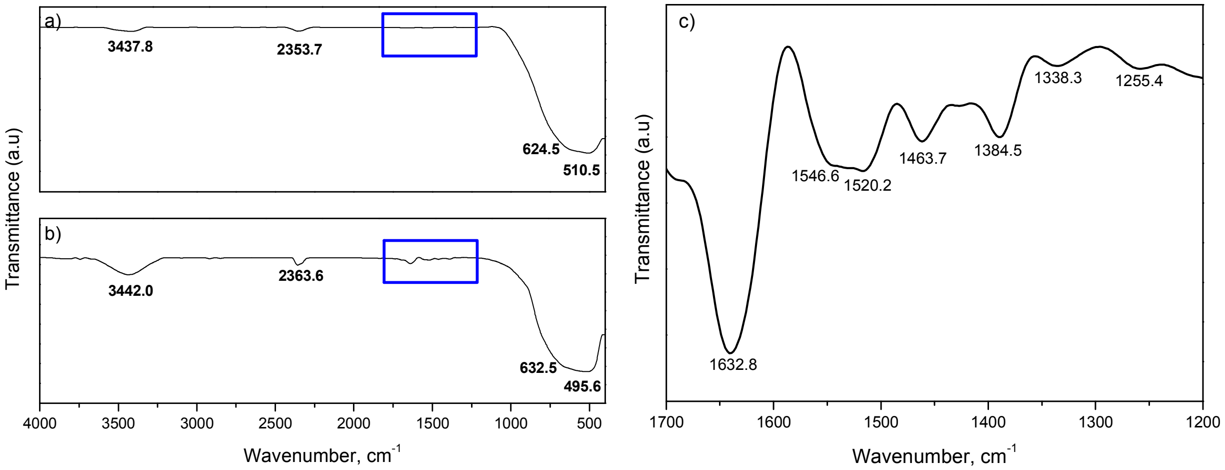

Fig. 10. FTIR spectra of a) N0-TiO_2, b) N1-TiO_2 and c) enlarged FTIR spectra of Fig. 10b) from 1200cm^{-1} to 1700 cm^{-1}

Fig. 11

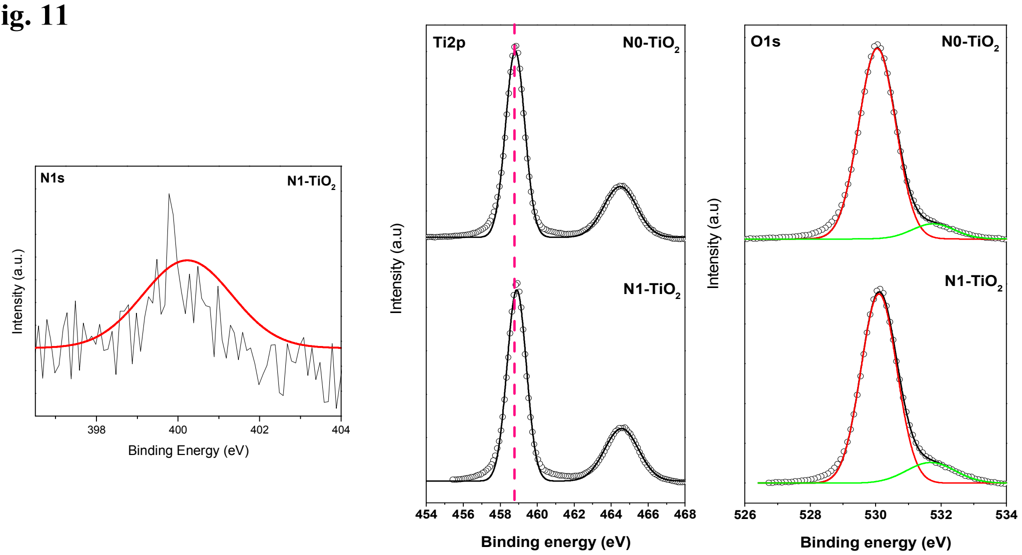

Fig. 11. XPS Spectra of N 1*s*, Ti 2*p* and O 1*s* of N0-TiO$_2$ and N1-TiO$_2$

Fig. 12

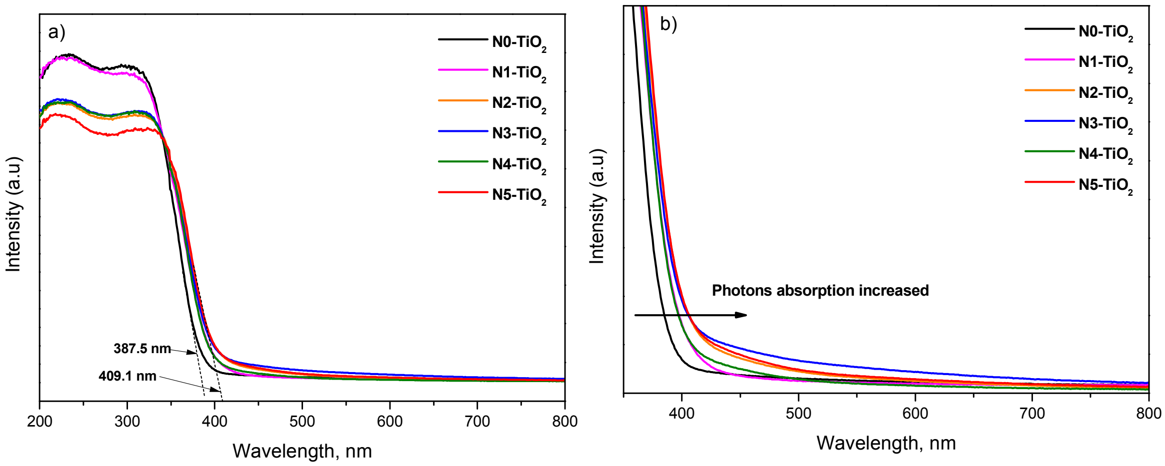

Fig. 12. a)Absorption spectrum and b) localized absorption spectrum for all prepared photocatalyst at different nitrogen loading

Fig. 13

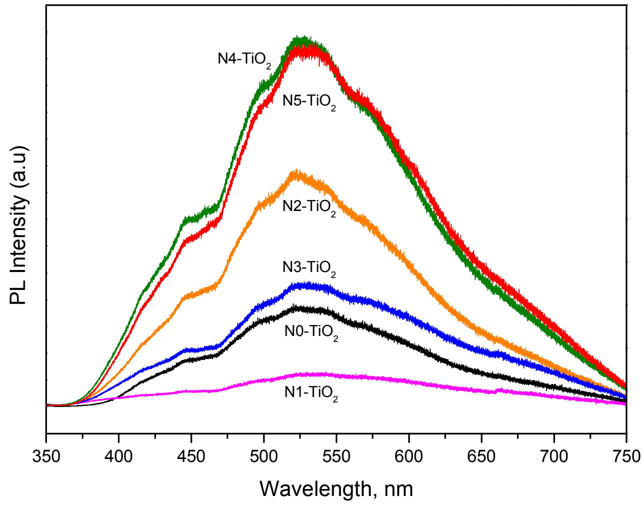

Fig. 13. Photoluminescence spectrum for for all prepared photocatalyst at different nitrogen loading

Fig. 14

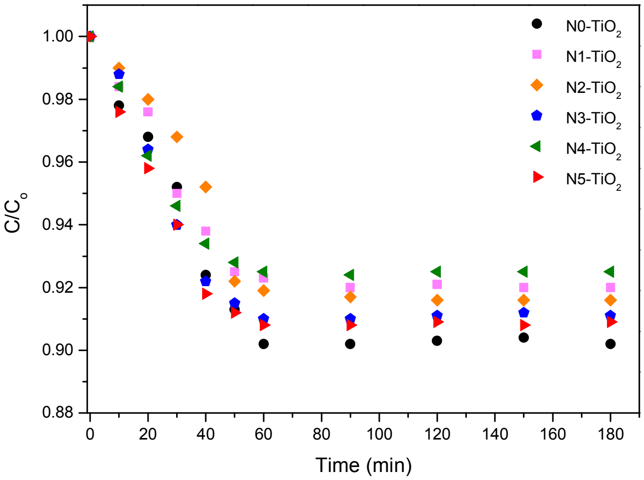

Fig. 14. Absorption-desorption profile of atrazine in darkness for all prepared photocatalyst at different nitrogen loading

Fig. 15

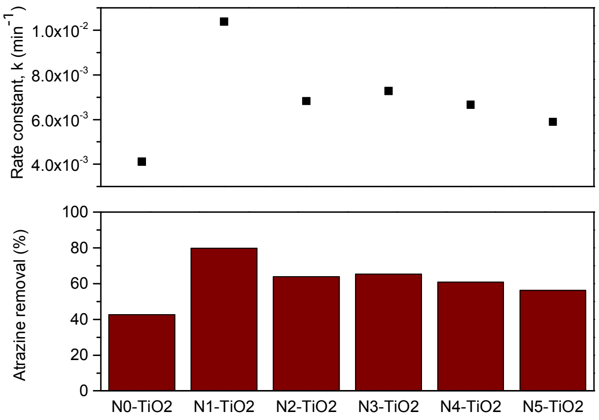

Fig. 15. Percentage removal of atrazine and its corresponding rate constant for all prepared photocatalyst at different nitrogen loading

Fig. 16

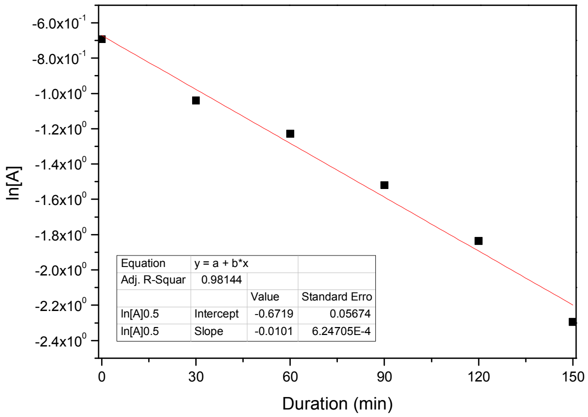

Equation	y = a + b*x		
Adj. R-Squar	0.98144		
		Value	Standard Erro
ln[A]0.5	Intercept	-0.6719	0.05674
ln[A]0.5	Slope	-0.0101	6.24705E-4

Fig. 16. First order rate of reaction graph of TiO_2 doped with nitrogen (r^2 coefficient > 98%)

Fig. 17

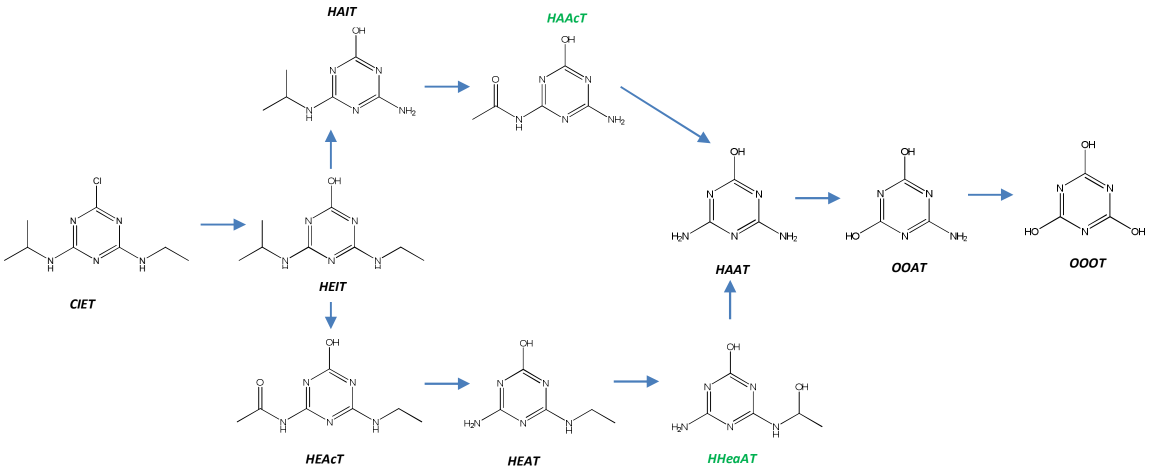

Fig. 17. Proposed degradation pathway of atrazine using TiO_2 doped with nitrogen
HAAct and HHeaAT were absence and not detected by LC/MS/MS

Caption of Tables

Table 1. Atomic and weight percentage of nitrogen in N-TiO_2

Table 2. Crystal structure, crystallite size, band gap, surface area and porosity of undoped and N-TiO_2

Table 3. Atrazine degradation intermediates by LCMS/MS

Table 1

Table 1. Atomic and weight percentage of nitrogen in N-TiO_2

[a]Initial N Molar Concentration	Sample Marking, NX-TiO_2	[b] Amount of N doped in TiO_2 (wt %)	[c] Amount of N doped in TiO_2 (wt %)
0.0	N0	0.00	0.00
0.5	N1	8.71	9.05
1.0	N2	10.32	11.03
1.5	N3	11.29	12.00
2.0	N4	13.99	13.71
2.5	N5	16.56	16.99

[a] Source of N from triethylamine precursor
[b] Amount of N successfully doped in TiO_2 (EDX analysis)
[c] Amount of N successfully doped in TiO_2 (CHNS analysis)

Table 2

Table 2. Crystal phase, crystallite size, band gap, surface area and porosity of undoped and N-TiO_2

Sample	Weight fractions of phase (%)		Average crystallite size, μm	d spacing	Band gap	BET surface area	Porosity
	Anatase	Rutile		Å	eV	m^2/g	cm^3/g
N0-TiO_2	94	6	23.0	3.50	3.20	48.98	0.235
N1-TiO_2	100	-	34.5	3.50	2.97	30.32	0.221
N2-TiO_2	100	-	34.5	3.50	2.93	26.61	0.245
N3-TiO_2	100	-	29.6	3.51	2.95	34.88	0.113
N4-TiO_2	100	-	29.6	3.51	2.97	38.78	0.134
N5-TiO_2	100	-	23.0	3.49	2.93	55.02	0.269

Table 3

Table 3. Atrazine degradation intermediates by LCMS/MS

Mass spectra, m/z[a]	Abbreviation	Compound
215.7	CIET	2-chloro-4-ethylamino-6-isopropylamino-s-triazine (atrazine)
197.3	HEIT	2-hydroxy-4-ethylamino-6-isopropylamino-s-triazine
197.2	HEAcT	2-hydroxy-4-ethylamino-6-acetamido-s-triazine
155.2	HEAT	2-hydroxy-4-ethylamino-6-amino-s-triazine
127.1	HAAT	2-hydroxy-4,6-diamino-s-triazine (ammeline)
169.2	HAIT	2-hydroxy-4-amino-6-isopropylamino-s-triazine
128.1	OOAT	2,6-hydroxy-4-amino-s-triazine (ammelide)
129.1	OOOT	2,4,6-triols-s-triazine (cyanuric acid)

[a] MS analysis in +ve ion mode